Polymer 50 (2009) 3016–3021

Contents lists available at ScienceDirect

Polymer

journal homepage: www.elsevier.com/locate/polymer

Affine deformation of single polymer chain in poly(methyl methacrylate) films under uniaxial extension observed by scanning near-field optical microscopy

Toru Ube [a], Hiroyuki Aoki [a,*], Shinzaburo Ito [a], Jun-ichi Horinaka [b], Toshikazu Takigawa [b], Toshiro Masuda [b]

[a] Department of Polymer Chemistry, Kyoto University, Nishikyo, Kyoto 610-8510, Japan
[b] Department of Material Chemistry, Kyoto University, Nishikyo, Kyoto 610-8510, Japan

ARTICLE INFO

Article history:
Received 24 February 2009
Received in revised form
22 April 2009
Accepted 26 April 2009
Available online 3 May 2009

Keywords:
Single polymer chain
Scanning near-field optical microscopy
Tensile deformation

ABSTRACT

The conformation of single poly(methyl methacrylate) chain in the uniaxially stretched film was observed by the combination of the fluorescence labeling technique and scanning near-field optical microscopy (SNOM). The dimension of the individual probe chain ($M_w = 1.99 \times 10^6$) along the extension axis was evaluated from SNOM image. In the high molecular weight matrix ($M_w = 1.89 \times 10^6$) the average extension ratio at the single chain level coincided with the macroscopic extension ratio. The distribution of the chain conformation was in good agreement with that of the freely jointed chain followed by affine deformation. On the other hand, the probe chain embedded in the low molecular weight matrix ($M_w = 1.76 \times 10^5$) showed the smaller extension than that expected from the affine deformation. This suggests that the conformation of the probe chain is affected by the relaxation of the short surrounding chains through disentanglement.

1. Introduction

The microscopic molecular structures of polymer chains such as orientation and conformation are closely related with macroscopic properties of polymer materials. Observing and controlling the chain structures are significant from both scientific and practical points of view. The stress induced by external deformation gives rise to the segmental orientation, which is observed by birefringence [1,2] and infrared absorption dichroism [1,3]. The stress-optical rule ensures the relationship between the chain motion and viscoelastic quantities. Abundant rheological studies have contributed to the developments of molecular models for the chain dynamics [4,5]. One of the most successful models for the entangled polymer system is the tube model developed by Doi and Edwards [6]. In this model, a tube along a certain chain is introduced to represent the topological constraint from the neighboring chains. It assumes the affine deformation under step strain and followed by reptation along the tube. The segmental orientation simulated under these microscopic assumptions well describes viscoelastic behavior. Further improvement of the model is performed by considering the relaxation of surrounding chains in terms of constraint release and dynamic tube dilation.

The theoretical models predict the chain motion not only in the segmental scale but also in the length scale of the whole single chain, which is characterized by parameters such as radius of gyration. The radius of gyration of a polymer chain in bulk systems has been experimentally investigated by small angle neutron scattering (SANS) [7]. Boué et al. studied the conformational change of polystyrene chains under uniaxial extension, concluding that the radius of gyration is affine soon after stretching for large enough chains [8–10]. The complementary observation in different length scales gives further insights of polymer dynamics. However, the segmental orientation and the radius of gyration obtained by the above methods are the averaged value for the numerous chains in the system, whereas the theoretical models are based on the behavior of single polymer chains. The observation of single polymer chains enables us to discuss the motion of individual chains in association with the variety of the chain conformation. The assumptions about the chain motion in the theoretical models are more clearly tested by observing individual properties of single polymer chains, which does not suffer from blur by averaging over a large number of chains.

In order to detect *in situ* features of polymer chains locating inside a bulk medium, a single chain must be distinguished from its surroundings. Fluorescence labeling is an established method, which has been applied to observe single DNA molecules. Chu et al. succeeded in the direct observation of the tube-like motion of DNA chains by fluorescence microscopy [11]. They also studied the conformational change of DNA molecules under elongational flow

* Corresponding author.
E-mail address: aoki@photo.polym.kyoto-u.ac.jp (H. Aoki).

0032-3861/$ – see front matter © 2009 Elsevier Ltd. All rights reserved.
doi:10.1016/j.polymer.2009.04.057

[12]. However, the conventional fluorescence microscopy suffers from the low spatial resolution due to the diffraction limit to a half of the wavelength of light. Therefore, the application of the optical microscopy to single macromolecular imaging has been limited to the observation of huge biomacromolecules such as DNA. Scanning near-field optical microscopy (SNOM) is an emerging scanning probe technique, which allows optical measurement with a high resolution beyond the diffraction limit of light [13–17]. The light incidence to the sub-wavelength-sized aperture generates an optical near-field restricted in the space of the aperture size. This allows one to illuminate the specimen and to obtain the optical response from the nanometric area. Therefore, SNOM enables us to directly observe the conformation of the single chain, which is fluorescently labeled and silhouetted against surrounding unlabeled polymers [18–22].

In the previous study, we showed that SNOM is a promising method to observe the elongated conformation of single polymer chains under the uniaxial deformation [20]. The chain conformation of poly(methyl methacrylate) (PMMA) was examined under the plastic deformation. We showed that the microscopic strain of the single chain was smaller than the macroscopic strain, suggesting the presence of slipping of polymer chain on the course of stretching. In the current study, we report the case of the elastic deformation. The PMMA films were uniaxially stretched above the glass transition temperature, quenched to room temperature, and then the conformation of the whole single chain was observed by SNOM. The chain deformations in different molecular weight matrices are discussed with the results of SNOM and birefringence.

2. Experiments

2.1. Sample preparation

The synthesis of perylene-labeled PMMA (PMMA-Pe, Fig. 1) is described elsewhere [22,23]. The fraction of the labeled unit was evaluated to be 0.77% by UV–Vis absorption (U3500, Hitachi). The unlabeled PMMAs with high and low molecular weight (denoted as PMMA-*h* and PMMA-*l*, respectively) were synthesized by atom transfer radical polymerization [24]. Methyl methacrylate was polymerized with *p*-toluenesulfonyl chloride in conjunction with copper(I) chloride and 4,4′-dinonyl-2,2′-dipyridyl at 70 °C in vacuum. The weight- and number-averaged molecular weights, M_w and M_n, of the polymers, which were determined by GPC measurement, are shown in Table 1.

In order to observe the single labeled chains in the PMMA bulk by SNOM, the sample containing a trace amount of PMMA-Pe near the surface was prepared in the following procedure. A mixed toluene solution of the unlabeled PMMA (PMMA-*h* or PMMA-*l*) and PMMA-Pe (0.005 wt.% to the unlabeled polymer) was spin-coated onto a glass substrate to form a film with a thickness of 80 nm. The thin film was floated onto a water surface and scooped up on a self-standing thick film of the unlabeled PMMA (the size was

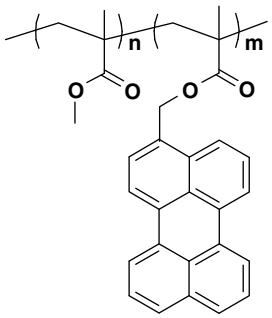

Fig. 1. Chemical structure of PMMA-Pe.

Table 1
Characterization of PMMA.

Sample	$M_w/10^6$	$M_n/10^6$	M_w/M_n
PMMA-Pe	1.99	1.58	1.26
PMMA-*h*	1.89	1.53	1.24
PMMA-*l*	0.176	0.132	1.33

25 mm × 7 mm, and the thickness was 300 μm), which was prepared separately by the solution casting. The conformation of PMMA-Pe may be affected by the shear flow in the spin-coating process and the confinement effect of the thin film. Therefore, the sample film was annealed for 48 h at 200 °C, which is longer than the relaxation time estimated from the literature [25], in vacuum to reach the equilibrium.

2.2. Tensile deformation

A tensile tester (RTM-500, Orientec) with a 10 kg load cell was used for stretching the films. The length between the clamps was 20 mm. The stretching was carried out at 160 °C with a crosshead speed of 5 mm/min. The force and displacement were monitored on a chart recorder. The extension ratio, λ, was calculated as l/l_0 where l_0 and l are the length of the film along the stretching direction before and after the elongation, respectively. The true stress, σ, was evaluated as follows assuming the constant volume of the film:

$$\sigma = \frac{F}{A} = \frac{F}{A_0}\lambda. \quad (1)$$

where F is the force applied to the sample, A is the sample cross section at the extension ratio of λ, A_0 is the cross section at $\lambda = 1$. After the stretching to the various extension ratios, the thermostatic chamber was opened and the film was rapidly cooled by the blow of air at room temperature. In this quenching procedure, the film was returned to the glassy state within 10 s.

2.3. Birefringence measurement

The birefringence measurement was carried out by Senarmont method. The optical system was composed of a laser, a polarizer, a quarterwave plate, an analyzer, and a photo detector. The axes of the polarizer and the quaterwave plate were set at 45° to the strain axis. After passing through the oriented sample, the plane polarized light becomes elliptically polarized. The quarterwave plate converts elliptical polarization into linear polarization with the azimuthal angle, α, which was determined by rotating the analyzer. The retardation, Γ, was evaluated as $\Gamma = \lambda_L(\alpha/\pi)$, where λ_L is the incident wavelength. The birefringence, Δn, was determined as $\Delta n = \Gamma/d$, where d is the sample thickness.

2.4. SNOM measurement

The SNOM measurement was performed by a commercially available instrument (α-SNOM, WITec) using a hollow cantilever probe with a sub-wavelength aperture of 60 nm. The laser beam at a wavelength of 438 nm (BCL-015-440, CrystaLaser) was focused onto the backside of the aperture to generate the optical near-field. While scanning the sample surface in the contact mode with the cantilever, the perylene fluorescence was collected by a microscope objective (0.80NA, 60×, Nikon) from the backside of the substrate, passed through a long-pass filter (AELP454, Omega Optical), and detected with a photomultiplier (H8631, Hamamatsu Photonics). The SNOM measurement was carried out in an ambient condition. All the SNOM images were taken by the same probe.

3. Results and discussion

Fig. 2 shows the true stress–extension ratio curves of the PMMA films stretched at 160 °C. Since the extension was carried out much above the glass transition temperature, the stress monotonously increased with the extension ratio. Fig. 3 shows the birefringence of the quenched film plotted against the extension ratio. Birefringence is related to the orientation of the chain segment as

$$\Delta n = \Phi \Delta n_0, \tag{2}$$

where Δn_0 is the intrinsic birefringence and Φ is an orientational order parameter

$$\Phi = \left(3\left\langle \cos^2\phi \right\rangle - 1\right)/2, \tag{3}$$

where ϕ is the angle between the stretching direction and the main axis of the structural unit, and $\langle\rangle$ represents the statistical average. The random orientation gives $\Phi = 0$, whereas the perfect uniaxial orientation gives $\Phi = 1$. The intrinsic birefringence of PMMA is reported as $\Delta n_0 = -0.0043$ [26]. Applying this value to our birefringence data, we calculated the orientational order parameter, which is shown in the right axis of Fig. 3. Under the assumption that each entanglement point changes its position affinely by the macroscopic deformation, the extension ratio dependence of Φ after the step strain is given from the rubber elasticity theory [27,28]:

$$\Phi = \frac{1}{5n}\left(\lambda^2 - \frac{1}{\lambda}\right), \tag{4}$$

where n denotes the number of segment between entanglements. We determined n from our experimental data of Φ in the early stage of the deformation. The dashed curve in Fig. 3 shows the theoretical curve obtained from Eq. (4) with $n = 6.7$. For the PMMA-*h* film, the experimental values of Δn ($\Phi = \Delta n/\Delta n_0$) almost agreed with the theoretical values based on the affine network model. The deviation at high extension ratios suggests that the segmental orientation of the polymer chain was somewhat relaxed during the extension process. The PMMA-*l* film showed smaller stress and birefringence compared with the PMMA-*h* film because the shorter chains relax more rapidly.

Fig. 4 shows the birefringence plotted against the stress. The birefringence was proportional to the stress according to the stress-optical rule [6],

$$\Delta n = C\sigma, \tag{5}$$

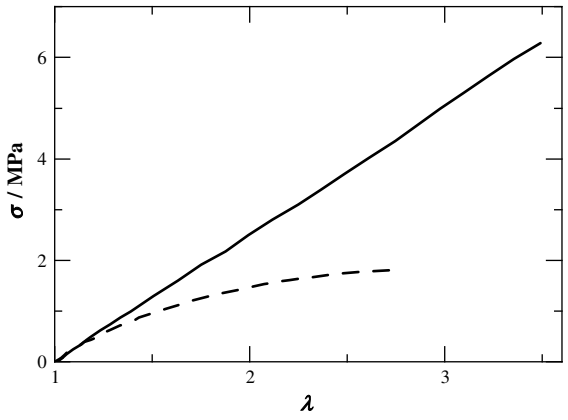

Fig. 2. True stress–extension ratio curves of PMMA-*h* and PMMA-*l* films (solid and dashed curves, respectively) stretched at 160 °C with a crosshead speed of 5 mm/min.

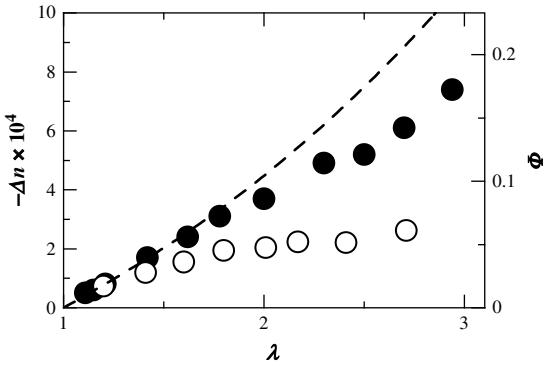

Fig. 3. Birefringence of the stretched PMMA films plotted against the extension ratio. Closed and open circles represent PMMA-*h* and PMMA-*l*, respectively. The right axis shows the orientational order parameter, and the dashed curve shows the calculated Φ value based on the affine network model (Eq. (4)).

where C is the stress-optical coefficient. This indicates that the stress is directly related to the orientation of the chain segment, not affected by the finite extensibility of the chain [29] and the glassy component [30] in our experimental condition. From Fig. 4, C was evaluated to be -1.5×10^{-10} Pa^{-1}, which is in good agreement with the values reported in the literature [1,2].

Fig. 5 shows the fluorescence SNOM images of the PMMA films under the uniaxial extension. The perylene-labeled PMMA chains embedded in the unlabeled bulk film were observed as the bright spots in the fluorescence image. Each fluorescence spot was confirmed to be individual PMMA-Pe chain from the statistical analysis [16]. Since the optical near-field penetrates into the sample film by a few hundred nm, the shape of the PMMA chain observed in the SNOM image is given as a two-dimensional projection of the chain conformation. In Fig. 5a, the single PMMA-Pe chains with the same molecular weight were observed in various forms, indicating the flexibility of the PMMA chain. Fig. 5b and c depicts the SNOM images of the films after stretching at the extension ratio of 2.0 and 3.0, respectively. These images clearly show the polymer chains with elongated conformations along the macroscopic stretching direction. We confirmed that the conformation of the whole single

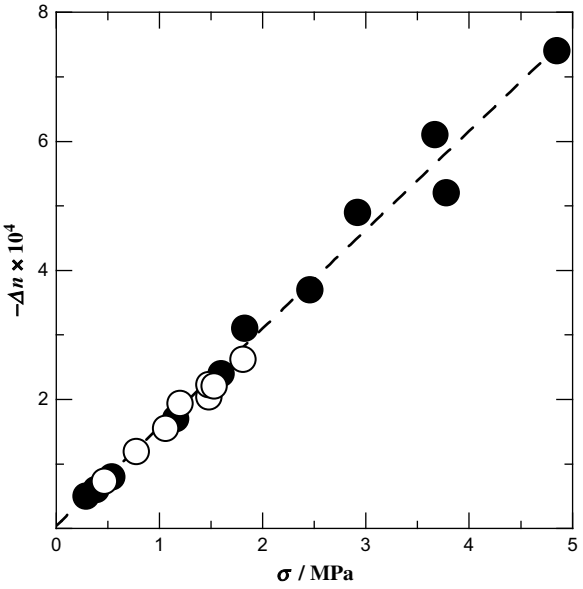

Fig. 4. Birefringence of the stretched PMMA films plotted against the stress. Closed and open circles represent PMMA-*h* and PMMA-*l*, respectively.

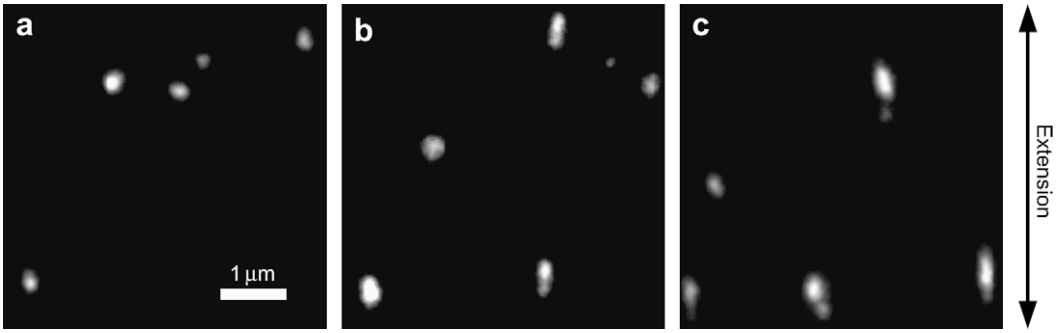

Fig. 5. Fluorescence SNOM images of single polymer chains in the PMMA-*h* films (a) before stretching, and after stretching to the extension ratio of (b) 2.0 and (c) 3.0.

chain does not change after relaxation periods of 10–60 s, therefore the conformation was not disturbed by the quenching process.

The conformation of the single PMMA chain was quantitatively evaluated from the fluorescence intensity distribution [21]. The fluorescence intensity is proportional to the number of fluorescence dye molecules randomly introduced to the PMMA-Pe chain; therefore, the intensity at each pixel is proportional to the number of the chain segment therein. The first moment of the fluorescence intensity distribution denotes the position of the center of mass,

$$\mathbf{r}_0 = \frac{1}{I}\sum_i \mathbf{r}_i I_i, \tag{6}$$

where I_i is the fluorescent intensity at the i-th pixel, $\mathbf{r}_i$ is the position vector, and I is the total fluorescence intensity from the single chain. The second moment of the fluorescence intensity distribution is calculated as

$$R_{xx}^2 = \frac{1}{I}\sum_i (x_i - x_0)^2 I_i, \tag{7}$$

$$R_{yy}^2 = \frac{1}{I}\sum_i (y_i - y_0)^2 I_i, \tag{8}$$

$$R_{xy}^2 = R_{yx}^2 = \frac{1}{I}\sum_i (x_i - x_0)(y_i - y_0) I_i, \tag{9}$$

where (x_i,y_i) and (x_0,y_0) are the position of the i-th pixel and the center of mass in the orthogonal coordinate system. We define the x axis as the macroscopic extension axis of the film. R_{xx} and R_{yy} indicate the dimensions of the fluorescence spot along the x and y axes, respectively. The tensor $\mathbf{R}$ is a parameter related to the polymer conformation,

$$\mathbf{R} = \begin{pmatrix} R_{xx}^2 & R_{xy}^2 \\ R_{yx}^2 & R_{yy}^2 \end{pmatrix}. \tag{10}$$

The eigenvalues λ_1 and $\lambda_2 (\lambda_1 > \lambda_2)$ of $\mathbf{R}$ correspond to the squared lengths of the long and short axes, respectively, of the most appropriate ellipsoid for the segmental distribution as shown in Fig. 6. The angle, θ, between the extension axis and the long axis of the ellipsoid is given by

$$\theta = \arctan\left(\frac{\lambda_1 - R_{xx}^2}{R_{xy}^2}\right). \tag{11}$$

In order to compare the conformational change of the polymer chains with the macroscopic extension ratio, we defined the extension ratio at the single chain level, λ_c, as

$$\lambda_c^2 = \frac{\left\langle R_{xx}^{*\,2}\right\rangle}{\left\langle R_{xx}^{*\,2}\right\rangle_0}, \tag{12}$$

where $\langle R_{xx}^{*2}\rangle_0$ and $\langle R_{xx}^{*2}\rangle$ denote the true average dimension of chains along the x axis before and after stretching as follows,

$$R_{xx}^{*\,2} = \frac{1}{N}\sum_j^N (x_j - x_0)^2, \tag{13}$$

where N is the number of segments and x_j is the x-coordinate of the position of the j-th segment of the chain [31]. Since the SNOM experiment suffered from the limit of resolution, which is caused by finite dimension of the aperture, the observed value of R_{xx} is somewhat larger than the true value, R_{xx}^*. The point spread function in fluorescence SNOM measurement is well approximated as a Gauss function, which was determined from the observation of a quantum dot [21]. Since the fluorescence from a single polymer chain is a sum of the fluorescence from the dye molecules, which is randomly distributed along the chain contour, the fluorescence image is expressed by the convolution of the distribution function of the chain segment and the point spread function. The variance of the convoluted function is sum of the variances of the original functions [32]. Therefore,

$$R_{xx}^2 = R_{xx}^{*\,2} + a^2, \tag{14}$$

where a^2 is the variance of the point spread function.

Fig. 7 shows the relationship between the extension ratio λ_c at the single chain and the ratio λ at the macroscopic level. As for the samples with the high molecular weight matrix, λ_c was almost equal

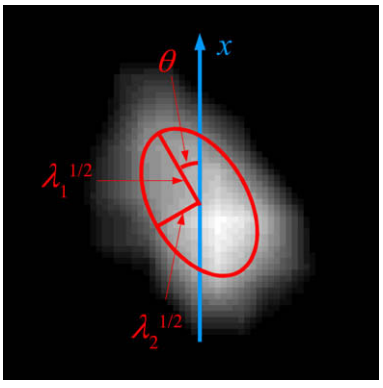

Fig. 6. An example of the analysis of a single fluorescence spot. The red curve shows the most appropriate ellipsoid for the segmental distribution.

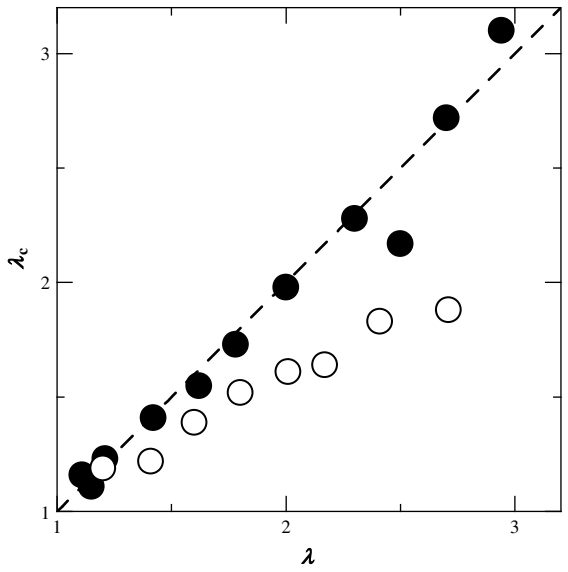

Fig. 7. Average chain extension ratio λ_c plotted against the macroscopic extension ratio λ of the film. Closed and open circles represent the samples with PMMA-*h* and PMMA-*l* matrices, respectively. The dashed line indicates the affine deformation ($\lambda_c = \lambda$).

to λ. This indicates the affine deformation of the single polymer chain in the sense that the dimension of the whole single chain changes in the same ratio as the macroscopic deformation of the film. It should be noted that SNOM and the birefringence have different length scale of the observation: SNOM measures the dimension of the whole contour of the single chain whereas the birefringence measures the orientation of the segment. As shown in Fig. 3, some parts of the segmental orientation is relaxed by the rearrangement in a relatively small length scale, which occurs within the time scale of the extension process. On the other hand, the relaxation of the chain dimension occurs by the motion of the whole chain contour, which is described as contraction and reptation in the tube model [6]. In our condition of the tensile deformation, the relaxation of the whole single chains hardly occurs during the extension process because of the large molecular weight of $M_w \simeq 2 \times 10^6$ compared with the molecular weight between entanglements, M_e, of PMMA; $M_e \simeq 4$–10×10^3 [33–35].

Next, we consider the extension of the chains embedded in the low molecular weight bulk medium. The labeled chains in the PMMA-*l* matrix showed smaller λ_c than λ. This is caused by the disentanglement of the matrix chain from the probe chain during the stretching of the film. Thus, the degree of the chain deformation depends on the molecular weight of the surrounding chains. The affine deformation of a whole chain is observed only when the rate of the disentanglement is much slower than the extension of the film.

We next discuss the conformation of individual polymer chains, taking the advantage of the single chain observation. Since we could not observe the same polymer chain before and after stretching due to the experimental difficulty, we discuss the distribution of the chain dimension along the extension axis normalized by its initial average, $R^*_{xx}/\langle R^*_{xx}\rangle_0$, and the angle θ between the main axis of the whole chain and the extension axis. Fig. 8 shows histograms of $R^*_{xx}/\langle R^*_{xx}\rangle_0$ for the samples with PMMA-*h* matrix ($\lambda = 1$, 2.0, and 3.0). The variety of the values results from the conformational distribution of the PMMA chains. The standard deviations of $R^*_{xx}/\langle R^*_{xx}\rangle_0$ were 0.43, 0.78, and 1.32 for the samples with $\lambda = 1$, 2.0 and 3.0, respectively. Fig. 9 shows histograms of θ for the same samples. It clearly shows that before stretching each chain was randomly oriented. After stretching, the orientation angle shows the narrow distribution with a peak at $\theta \sim 0^\circ$. This indicates that the PMMA chains in the elongated film take a stretched conformation along the elongation axis. The distribution of θ narrowed with the increase of the macroscopic strain. The standard deviations of θ were 48.1, 21.8, 12.5 for the samples with $\lambda = 1$, 2.0 and 3.0, respectively. We compared the experimental values of $R^*_{xx}/\langle R^*_{xx}\rangle_0$ and θ with those obtained from the random walk simulation. The freely jointed chains were generated in three-dimensional space by Monte Carlo method. In the simulation of the uniaxial extension of the film, the affine deformation of the all segment was

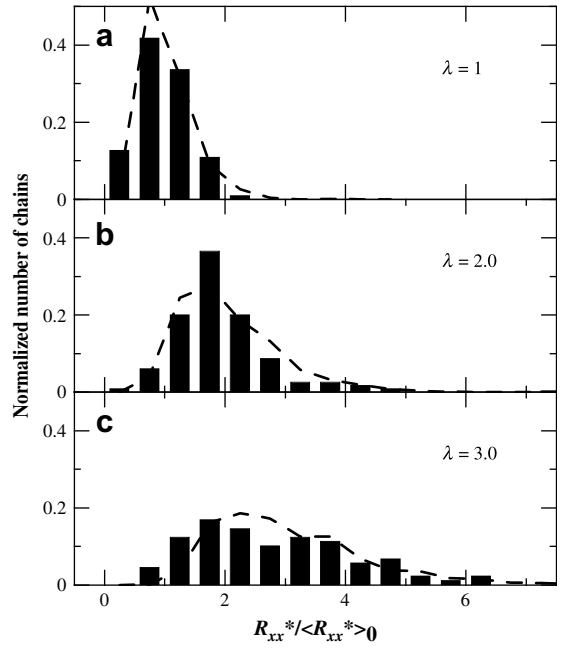

Fig. 8. Histograms of the chain dimension parallel to the stretching direction normalized by the initial average value in the film (a) before stretching, and after stretching to the extension ratio of 2.0 and 3.0. The matrix is PMMA-*h*. The dashed lines indicate the results of random walk simulation followed by affine deformation.

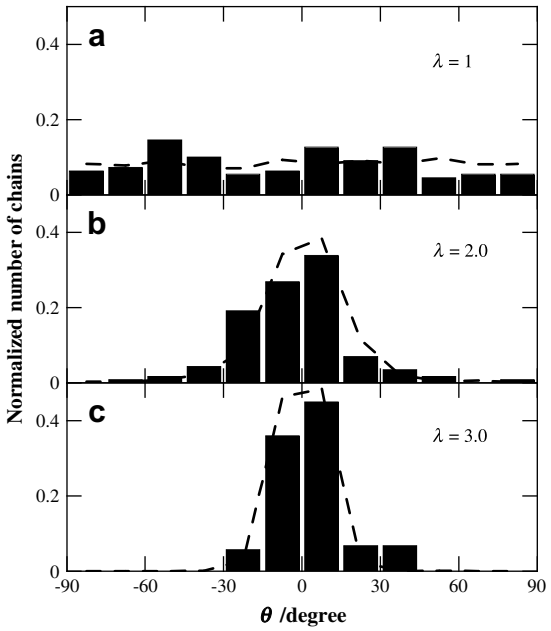

Fig. 9. Histograms of the orientation of the PMMA chain to the stretching direction of the film (a) before stretching, and after stretching to the extension ratio of 2.0 and 3.0. The matrix is PMMA-*h*. The dashed lines indicate the results of random walk simulation followed by affine deformation.

assumed. R^*_{xx} was calculated from Eq. (13) for each generated chain. θ was also determined by the same procedure as Eq. (11). The dashed lines in Figs. 8 and 9 show the results of the random walk simulation. Both of the experimentally obtained histograms for $R^*_{xx}/\langle R^*_{xx}\rangle_0$ and θ were in good agreement with the random walk simulation on the basis of the affine deformation not only for the average value but also for the distribution function. This indicates that the polymer chain with a large molecular weight deforms according to the affine transformation at the single chain level.

4. Conclusion

SNOM was applied to observe the single polymer chains embedded in the PMMA films, which were stretched much above the glass transition temperature. For the samples with the high molecular weight matrix, the average chain extension ratio coincided with the macroscopic extension ratio, showing the affine deformation of the whole chain, whereas the segmental orientation evaluated from birefringence was smaller than that expected from the affine network model. Thus, the extension of the polymer chain depends on its length scale of the observation. In the low molecular weight matrix, the chain extension ratio was smaller than the macroscopic extension ratio, which is caused by the disentanglement of the short matrix chain from the probe chain. The variety of the single chain conformation was analyzed in terms of the chain dimension along the extension axis, and the angle between the main axis of the whole chain and the extension axis. For the sample with high molecular weight matrix, these parameters almost agreed with those obtained from random walk simulation followed by affine deformation not only for the average value but also for the distribution.

Acknowledgement

This work is supported by Grants-in-Aid from Japan Society for the Promotion of Science (JSPS) and from Ministry of Education, Culture, Sports, Science and Technology, Japan (MEXT). The authors acknowledge also the Innovative Techno-Hub for Integrated Medical Bio-imaging Project of the Special Coordination Funds for Promoting Science and Technology from MEXT.

References

[1] Kahar N, Duckett RA, Ward IM. Polymer 1978;19:136–44.
[2] Marrucci G, de Cindio B. Rheol Acta 1980;19:68–75.
[3] Zhao Y, Jasse B, Monnerie L. Makromol Chem Macromol Symp 1986;5:87–97.
[4] Watanabe H. Prog Polym Sci 1999;24:1253–403.
[5] McLeish TCB. Adv Phys 2002;51:1379–527.
[6] Doi M, Edwards SF. The theory of polymer dynamics. Oxford: Clarendon; 1986.
[7] Cotton JP, Decker D, Benoit H, Farnoux B, Higgins J, Jannink G, et al. Macromolecules 1974;7:863–72.
[8] Boué F. Adv Polym Sci 1987;82:47–101.
[9] Picot C, Duplessix R, Decker D, Benoit H, Boué F, Cotton JP, et al. Macromolecules 1977;10:436–42.
[10] Boué F, Nierlich M, Jannink G, Ball R. J Phys (Paris) 1982;43:137–48.
[11] Perkins TT, Smith DE, Chu S. Science 1994;264:819–22.
[12] Smith DE, Chu S. Science 1998;281:1335–40.
[13] Betzig E, Trautman JK. Science 1992;257:189–95.
[14] Ohtsu M, editor. Near-field nano/atom optics and technology. Tokyo: Springer; 1998.
[15] Aoki H, Ito S. J Phys Chem B 2001;105:4558–64.
[16] Aoki H, Kunai Y, Ito S, Yamada H, Matsushige K. Appl Surf Sci 2002;188:534–8.
[17] Ito S, Aoki H. Bull Chem Soc Jpn 2003;76:1693–705.
[18] Ito S, Aoki H. Adv Polym Sci 2005;182:131–69.
[19] Aoki H, Anryu M, Ito S. Polymer 2005;46:5896–902.
[20] Ube T, Aoki H, Ito S, Horinaka J, Takigawa T. Polymer 2007;48:6221–5.
[21] Yang J, Sekine R, Aoki H, Ito S. Macromolecules 2007;40:7573–80.
[22] Aoki H, Morita S, Sekine R, Ito S. Polym J 2008;40:274–80.
[23] Aoki H, Tanaka S, Ito S, Yamamoto M. Macromolecules 2000;33:9650–6.
[24] Grimaud T, Matyjaszewski K. Macromolecules 1997;30:2216–8.
[25] Masuda T, Kitagawa K, Onogi S. Polym J 1970;1:418–24.
[26] Kashiwagi M, Folks MJ, Ward IM. Polymer 1971;12:697–710.
[27] Treloar LRG. The physics of rubber elasticity. 3rd ed. Oxford: Clarendon; 1975.
[28] Roe RJ, Krigbaum WR. J Appl Phys 1964;35:2215–9.
[29] Matsumoto T, Bogue DC. J Polym Sci Polym Phys Ed 1977;15:1663–74.
[30] Inoue T, Okamoto H, Osaki K. Macromolecules 1991;24:5670–5.
[31] Rudnick J, Gaspari G. Science 1987;237:384–9.
[32] Laury-Micoulaut CA. Astron Astrophys 1976;51:343–6.
[33] Ferry JD. Viscoelastic properties of polymers. 3rd ed. New York: Wiley; 1980.
[34] Fetters LJ, Lohse DJ, Richter D, Witten TA, Zirkel A. Macromolecules 1994;27:4639–47.
[35] Fuchs K, Friedrich C, Weese J. Macromolecules 1996;29:5893–901.